Journal of Hydrology 612 (2022) 128075

Contents lists available at ScienceDirect

Journal of Hydrology

journal homepage: www.elsevier.com/locate/jhydrol

Research papers

Flood inundation in the Lancang-Mekong River Basin: Assessing the role of summer monsoon

Jie Wang[a,b], Qiuhong Tang[a,b,*], Xiaobo Yun[a,b], Aifang Chen[c], Siao Sun[b,d], Dai Yamazaki[e]

[a] Key Laboratory of Water Cycle and Related Land Surface Processes, Institute of Geographic Sciences and Natural Resources Research, Chinese Academy of Sciences, Beijing, China
[b] University of Chinese Academy of Sciences, Beijing, China
[c] School of Environmental Science and Engineering, Southern University of Science and Technology, Shenzhen, China
[d] Key Laboratory of Regional Sustainable Development Modeling, Institute of Geographic Sciences and Natural Resource Research, Chinese Academy of Sciences, China
[e] Global Hydrological Prediction Center, Institute of Industrial Science, The University of Tokyo, Komaba, Tokyo, Japan

ARTICLE INFO

This manuscript was handled by Marco Borga, Editor-in-Chief, with the assistance of Yadu Pokhrel, Associate Editor

Keywords:
Inundation characteristics
Indian Summer Monsoon
Western North Pacific Monsoon
Monsoon combined effect
Lancang-Mekong River Basin

ABSTRACT

Although it is well known that precipitation and flood pulses in the Langcang-Mekong River Basin (LMRB) are largely impacted by monsoons, it is unclear to what extent flood inundation characteristics (i.e., inundation frequency, depth, area, and timing) in the basin respond to different monsoon types and monsoon combined effect, i.e., the Indian summer monsoon (ISM), the Western North Pacific Monsoon (WNPM), and their combined effect (ISWN). In this study, flood inundation in the LMRB during 1967–2015 was simulated by a hydrological-hydrodynamic model, from which the inundation characteristics were extracted and calculated. The monsoon impact on inundation characteristics was then quantified using the slope from linear regression model. The results show the monsoons and the ISWN overall have a positive impact on inundation frequency, depth, and area, while the inundation timing is usually advanced when the WNPM or the ISWN strengthens but delayed when the ISM strengthens. On average, a unit change in different monsoons can cause, 7.7%–14.2% change in inundation frequency, 5.3%–8.1% change in inundation depth and 4.3 days–5.8 days change in inundation timing for depth, which can also lead to 1.0%–4.3% change in inundation area and 2.8 days–3.8 days change in inundation timing for area. Also, the relative contributions of different monsoons and spatial distributions of the dominant monsoon were discussed. The results indicate different monsoons regulate different inundation characteristics, and suggest the coexistence of monsoon impacts. If the impact of the ISWN is ignored, the WNPM will play a more important role than the ISM in affecting the inundation.

1. Introduction

The Lancang-Mekong River Basin (LMRB) is one of the few flood-prone areas in Asia with the highest worldwide fatality rates induced by flooding (Chen et al., 2020). A significant increase in basin-wide temperature and changes in monsoon patterns have been projected by climate models (e.g., Pokhrel et al., 2018), and it is expected to cause increases in extreme rainfall, which could ultimately drive changes in flood regime of the basin (e.g., Lauri et al., 2012; Wang et al., 2017). Thus, understanding the flood dynamics under climate change in this basin is crucial to its future water resource and flood risk management.

Up to now, a series of studies, including historical flood evolution (e.g., Delgado et al., 2010; Pokhrel et al., 2018; Chen et al., 2020) and future flood projections (e.g., Lauri et al., 2012; Hoang et al., 2016; Wang et al., 2017; Try et al., 2020a, b), have shown signals of increasing floods in the LMRB. Delgado et al. (2010) found the flood frequency increased during the last half century. Chen et al. (2020) also showed both the flood occurrence and maximum magnitude significantly increased during 1985–2018. Based on the future climate scenarios, Try et al. (2020a, b) predicted that the more severe flood magnitudes than under current climate conditions would occur by the end of this century, which might cause up to 43% and 55% increases in inundation area and inundation volume, respectively. With the likelihood of increasing floods in the LMRB, it is important to understand how climate change affects the flood regime.

Typically, climate change affects flood mainly by rainfall. The

* Corresponding author at: Key Laboratory of Water Cycle and Related Land Surface Processes, Institute of Geographic Sciences and Natural Resources Research, Chinese Academy of Sciences, Beijing, China.
E-mail address: tangqh@igsnrr.ac.cn (Q. Tang).

https://doi.org/10.1016/j.jhydrol.2022.128075
Received 17 September 2021; Received in revised form 23 May 2022; Accepted 7 June 2022
Available online 18 June 2022

anomalies in atmospheric general circulation such as monsoon changes can cause regional rainfall change (e.g., Yang et al., 2019). Increasing moisture in the atmosphere due to global warming, could also lead to an increase in magnitude and frequency of rainfall (e.g., Kunkel et al., 2013). In the LMRB (Fig. 1a), a monsoonal climate with distinct wet and dry seasons dominates its hydro-climate conditions (e.g., Yang et al., 2019). Over 80% of annual precipitation and 80%–90% of discharge occur during May to October, which can be attributed to the monsoon (Costa-Cabral et al., 2008; Delgado et al., 2012). Therefore, flood in this basin is mainly dominated by monsoon induced rainfall, with other sources being snowmelt from the Tibetan Plateau and localized tropical storms (Delgado et al., 2012).

In general, the Indian summer monsoon (ISM) and Western North Pacific Monsoon (WNPM) are two systems regulating the monsoon rainfall in the LMRB (e.g., Ding and Chan, 2005; Delgado et al., 2012). The rainy season precipitation in the west of LMRB is significantly influenced by the ISM, while that in the southeastern LMRB is significantly affected by the WNPM (Yang et al., 2019). Significant positive correlations between rainfall and the WNPM and ISM were found over 29.3% and 12.8% regions in the LMRB, respectively (Fan and Luo, 2019). More importantly, it was found that the interannual variability of the rainy season precipitation in the LMRB is significantly modulated by the combined effect of the ISM and WNPM (e.g., Yang et al., 2019). A positive correlation between rainfall and the combined effect of two monsoons was obtained in the LMRB (Yang et al., 2019). Further, studies on the monsoon impact on rainfall were also extended to the impact on discharge. Xue et al. (2011) reported the ISM impacts on annual mean discharge in the middle to lower reaches of the Mekong River. A positive relationship between the WNPM and discharge averaged from June to November in the southern LMRB regions was found by Delgado et al. (2012). Similar results were also reported by Fan and Luo (2019), where they showed the downstream river flow from June to September is modulated by the WNPM.

In addition to the studies of monsoon impacts on rainfall and discharge, the study of monsoon impacts on flood pulse characteristics across the LMRB was caried out by Wang et al. (2022). It was found that the flood start date was advanced, while Q_{10} and flood volume increased during the strong monsoon years. However, the flood represented by discharge in Wang et al. (2022) does not necessarily provide valuable information on the damage caused by flood, which is due to the fact that river characteristics, such as the river channel passing capacity at different locations, can significantly affect the flood damage. Instead, the flood represented by inundation, a visual response of water level/discharge to heavy storms and critical to the social damage of the flood, can provide more information on flood damage. Nevertheless, few studies have assessed the monsoon impact on inundation. It is still unclear how monsoons affect inundation in the LMRB, which is important to the research of climate related disasters in the basin.

Usually, there are several approaches available for assessing the monsoon impact on flood. Observation, in particular, is a commonly used method to analyze the monsoon impact on flood. Delgado et al. (2012) and Räsänen and Kummu (2013) have separately studied the impacts of monsoons and El Niño-Southern Oscillation on flood, where the in-situ flood discharges upstream of the Cambodian and Vietnamese Mekong River floodplains (i.e., the Cambodian and Vietnamese parts of the LMRB, CVM) were focused. Chen et al. (2021) also used observed water level in the Tonle Sap Lake (TSL) to analyze the impacts of El Niño-Southern Oscillation, Pacific Decadal Oscillation and the Indian Ocean Dipole on flood pulse parameters. However, the analyzes based on observation are hard to extend across the whole river basin due to the limited in-situ stations. Assessment of the impacts of climate variables, such as the summer monsoon, on flood could also be biased if limited in-situ stations were used (Wang et al., 2022). Further, remote sensing can also be used to analyze the monsoon impact on flood at regional scales, but it suffers from data deficiencies due to the issues of the satellite repeat cycle, cloud cover and vegetation (e.g., Ji et al., 2018; Boergens et al., 2019; Shin et al., 2020). Hydrological models can provide basin-wide discharge, which can further provide inundation by a discharge rating curve, but this is not an ideal tool for flood inundation due to the backwater effect and channel bifurcation in the lower floodplain (e.g., CVM). In particular, a unique flow reversal between the TSL and the Mekong River mainstream is formed during May to September (Kummu et al., 2014), making the hydrological regime more complex. A hydrodynamic model considering the backwater effect and channel bifurcation is therefore needed to simulate flood inundation in this basin.

In view of the research gap identified above (i.e., unclear knowledge

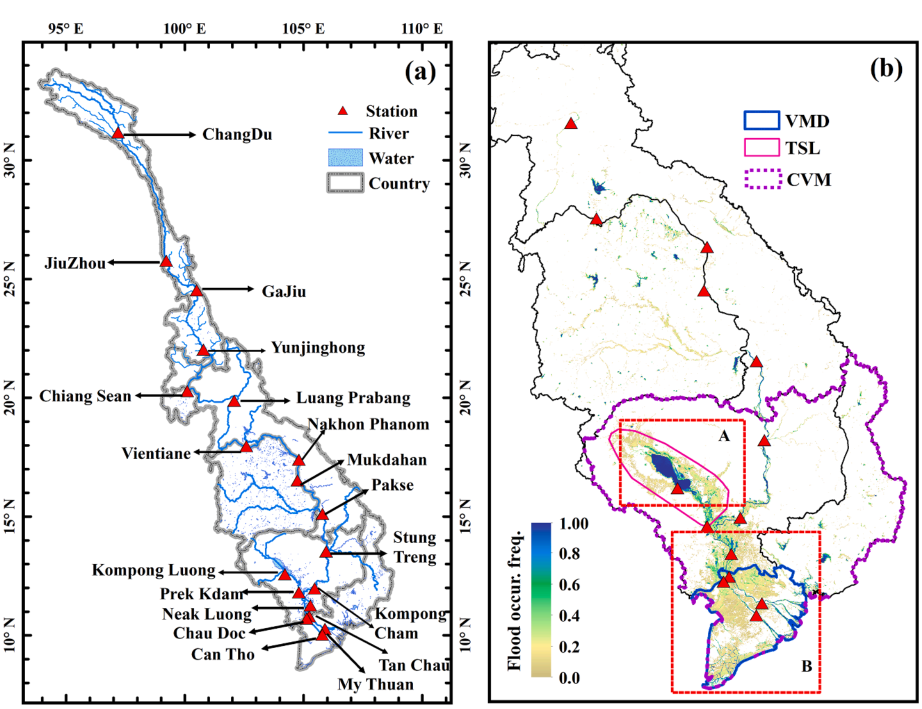

Fig. 1. Overview of the Lancang-Mekong River Basin (LMRB, a), and the distribution of daily flood occurrence frequency during June-November in 2001–2015 (b) using the Moderate-Resolution Imaging Spectrometer postprocessing product (MODIS, see Ji et al., 2018). The frequently flooded regions are mainly in regions A (Tonle Sap Lake, TSL, Kummu et al., 2014) and B (Vietnamese Mekong Delta, VMD, Minderhoud et al., 2019), which are both located in Cambodian and Vietnamese parts of the LMRB (CVM). Nineteen hydrological stations were used for model calibration and validation (a).

of monsoon impacts on flood inundation) and approach available (i.e., hydrodynamic modeling), this study aims to analyze the monsoon impact on flood inundation (i.e., inundation depth, frequency, area, and timing) in the LMRB with a special focus on the CVM regions (i.e., the frequently flooded regions in the basin, Fig. 1b). A hydrodynamic model was used to generate flood inundation characteristics, with monsoons indices collected and calculated to represent the monsoon strengths. Then the slope from linear regression was used to quantify the monsoon impact on inundation characteristics. The relative contributions of the monsoon to flood inundation and spatial distributions of the dominant monsoon (i.e., the monsoon with the largest contribution to inundation) in affecting flood inundation were also discussed.

2. Data and methods

2.1. Model description

The Catchment-Based Marco-scale Floodplain model (CaMa-Flood, v3.6.2, Yamazaki et al, 2013) considering the regional parameterization (Wang et al., 2021) was used to simulate flood inundation depth at 500 m spatial resolution, with a Variable Infiltration Capacity (VIC, v4.20d, Liang et al., 1994, Liang et al., 1996) model providing runoff at a spatial resolution of $0.25^{\circ} \times 0.25^{\circ}$ as the input. The meteorological forcing data including precipitation, temperature, and wind speed during the period from 1961 to 2015 to run the VIC model were collected from CN05.1 (Wu and Gao, 2013), Asian Precipitation-Highly Resolved Observational Data Integration Toward the Evaluation of Water Resource (Yatagai et al, 2009) and Princeton hydrological dataset (Sheffield et al., 2006). The spin-up period for both models was 1961–1966, while the calibration period was set to 1967–2007. In-situ water level and discharge series at Nineteen hydrological stations (see Fig. 1 for the gauging station spatial distribution), mainly collected from Henck et al. (2011), Mohammed et al. (2018), Annual Hydrological Reports of China, and Mekong River Commission, were used to calibrate the model parameters. Further details on model inputs, calibration, and model settings are given in Wang et al. (2021). The daily Moderate Resolution Imaging Spectrometer based water surface database (MODIS, Ji et al., 2018) from 2001 to 2015, and monthly Landsat based Global Surface Water dataset (GSW, Pekel et al., 2016) from 1987 to 2015 were also collected as flood inundation validation datasets. Here, since these two remote sensing datasets do not contain inundation depth information, floodplain with an inundation depth over 0.1 m and river channel in the model were considered to be inundated to make full comparisons with MODIS and GSW by following Wang et al. (2021). The Nash-Sutcliffe efficiency coefficient, Pearson correlation coefficient and relative error were used to assess the model performance at gauging stations. Because of the impacts caused by cloud, vegetation cover, and the satellite repeat cycle (e.g., Ji et al., 2018; Boergens et al., 2019; Shin et al., 2020), only the probability of detection, based on Wu et al. (2014), was calculated to evaluate the model performance in simulating flood inundation during the flood season. Here, the probability of detection was defined as the ratio of the simultaneous inundation occurrence frequency (i.e., the number of inundation days) which occurred for both the model and remote sensing dataset (MODIS or GSW), to the inundation occurrence frequency that occurred for the remote sensing dataset. Referring to Delgado et al. (2012) and Triet et al. (2020), the flood season was defined as a period from June to November, and the non-flood season was from December to May.

2.2. Monsoon index

Daily monsoon index data based on the definition of Wang et al. (2001) were collected from the Asia-Pacific Data-Research Center. The mean value of this index data from June to September each year was then calculated to represent the monsoon intensity for each year. A simple sum of the ISM and WNPM indices with the same weights developed by Yang et al. (2019) was also adopted to characterize the monsoon combined effect (ISWN, the abbreviation of ISM–WNPM, assumed to be a monsoon for an easier description hereafter). These three monsoon indices were then normalized (see Fig. 2) and used to analyze the monsoon impact on flood inundation.

2.3. Inundation characteristics

The inundation in the flood season was considered in this study. A grid for floodplain or river channel with the simulated inundation depth of 0.50 m or greater was thought to be inundated catastrophically, and was used for the analyses of monsoon impact in the following. This threshold of 0.50 m for flood inundation has also been used by Try et al. (2018), Try et al. (2020c) and Triet et al. (2018), Triet et al. (2020). Four inundation characteristics were used: frequency, depth, area, and timing (for flood peak). The first two and the third one were addressed at grid and regional scales, respectively; while the last one was considered both at grid and regional scales. The inundation frequency for a year was defined as the ratio of days with inundation to the whole duration of the flood season. The variables for inundation depth are the average inundation depth and maximum inundation depth, which were defined as the annual mean and maximum values of inundation depths, respectively. Similarly, two variables characterizing the inundation area, i.e., mean inundation area and maximum inundation area, were separately defined as the annual mean and maximum values of inundation areas, and calculated year after year. Here, the inundation area for a particular day was calculated as the sum of the grid areas for grids that are inundated. Two inundation timing variables (i.e., depth and area) were also considered in this study, i.e., the maximum inundation depth time (i.e., the day of the year that the maximum inundation depth occurs) at grid scale, and the maximum inundation area time (i.e., the day of the year that the maximum inundation area occurs) at regional scale, where the inundation timing for area was analyzed in the characteristic of inundation area for convenience.

2.4. Analysis of monsoon impact

The p-value calculated from a significance test of the Pearson correlation coefficient between the inundation variable and monsoon index (two-tailed t-test) was adopted to characterize the monsoon impact on inundation. Referring to the practice of the definition of monsoon anomaly (e.g., Wang et al., 2001; Li et al., 2016), which treats the monsoon as strong or weak when the normalized monsoon index exceeds one standard deviation (σ), a p-value of 0.32 (0.146 for Pearson correlation coefficient in this paper) corresponding to one σ criteria, was used as the threshold of the monsoon impact on inundation. This option considered the model capacity in modeling the floods, where the floods are the high value parts of discharge/water level and are always underestimated in modeling practice (e.g., Wang et al., 2021). When the p-value in a given region is no more than 0.32, the impact of monsoon on inundation in this region exists and this region can be treated as a monsoon impact region; otherwise, the impact is ignored. Delgado et al. (2012) also thought that a station with Pearson correlation coefficient less than 0.1 meant the flood in this station was not affected by the monsoon. In addition, regions with p-values no more than 0.05 and 0.10, generally used to indicate significance, were also marked to reflect a significant impact of the monsoon on inundation, but only the results of p-values no more than 0.05 were presented in the results for reference.

The slope from the linear regression model (Eq. (1), Hameed et al., 1997) was used to obtain the inundation response to one unit change in the monsoon index:

$$y = ax + b + \varepsilon \tag{1}$$

where y is the inundation variable (e.g., depth, frequency), x is the normalized monsoon index. a, b are the slope and constant, respectively.

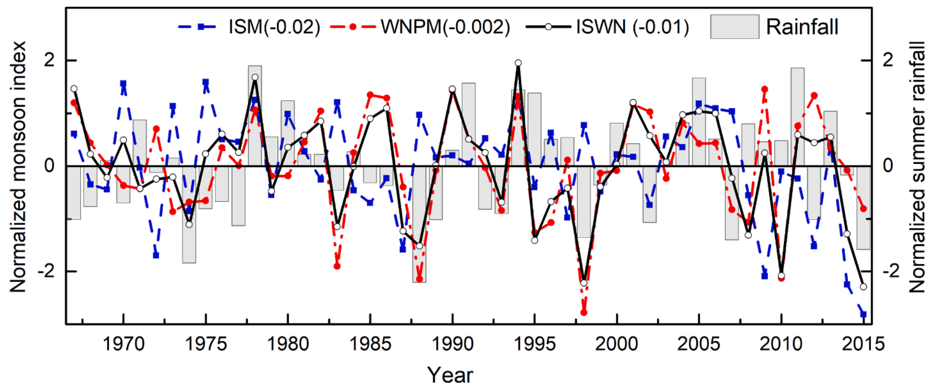

Fig. 2. Normalized summer monsoon indices and normalized basin average summer rainfall (June to September) between 1967 and 2015. Indian Summer Monsoon (ISM), Western North Pacific Monsoon (WNPM) and their combined effect ISWN were illustrated. The number in parentheses is the slope of monsoon index during 1967–2015.

ε is the error. If the slope is positive (or negative), then the monsoon impact on inundation is considered positive (or negative), that is, the inundation increases (or decreases) when the monsoon strengthens (i.e., monsoon index increases). To characterize the percentage change of inundation, the long-term average value was used, which was calculated as the average value of the inundation variable for the days with inundation. Then the slope dividing by the long-term average value was taken as the percentage change of flood inundation (see Eq. (2)):

$$\frac{y - y_{avg}}{y_{avg}} = \frac{a}{y_{avg}}x + \left(\frac{b}{y_{avg}} - 1\right) + \varepsilon \tag{2}$$

in which y_{avg} is the long-term average value, a/y_{avg} was the percentage change of flood inundation. A multi-linear regression model (Eqs. (3)–(4), Üneş et al., 2020) was also used to characterize the relative contributions of monsoons to inundation, and identify the spatial distribution of the dominant monsoon (i.e., the monsoon with largest relative contribution) in affecting inundation:

$$y = \sum_{i=1}^{n} a_i x_i + a_0 + \varepsilon \tag{3}$$

$$r_i = \frac{|a_i|}{\sum_{i=1}^{n}|a_i|} \tag{4}$$

where a_i ($i = 0,1, \ldots, n$) is the regression coefficient, x_i, r_i ($i = 1, 2, 3$ for this issue) are the normalized monsoon index and relative contribution for each x_i, respectively. y is the inundation variable. A similar approach has also been applied by Wang et al., (2020). Here, if the monsoon impact on inundation does not exist (i.e., p-value over 0.32), then this type of monsoon was excluded in the multi-linear regression analysis. Note that the ISWN index is a simple sum of the ISM and WNPM indices, though it was normalized before analysis (see section 2.2), suggesting

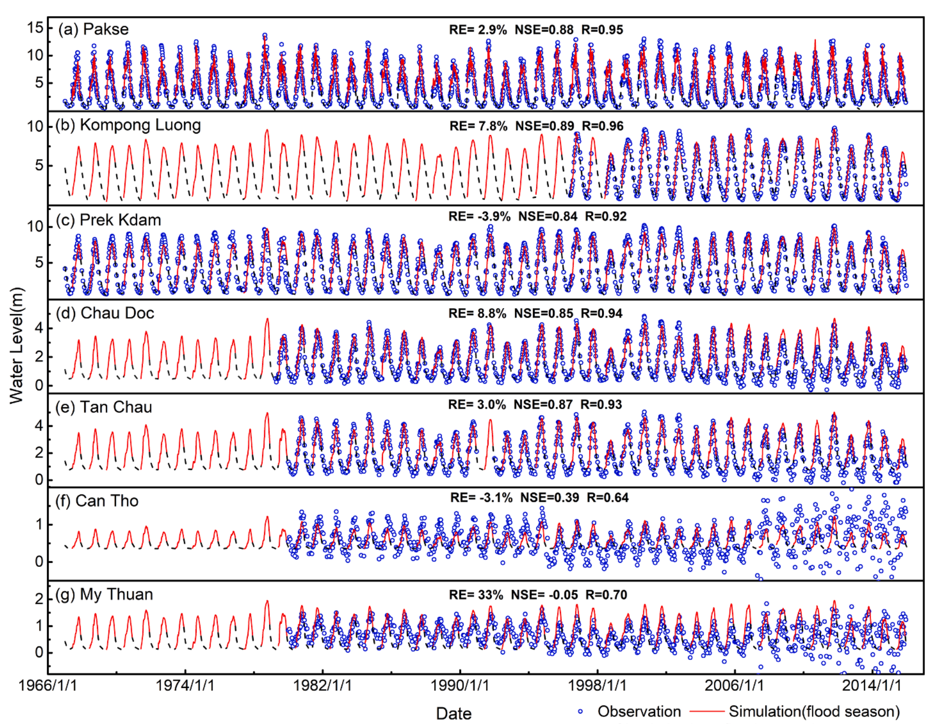

Fig. 3. Flood season water level simulations in comparison with observations around the frequently flooded regions (a-d). "*RE*", "*NSE*" and "*R*" represent the relative error, Nash-Sutcliffe efficiency coefficient, and Pearson correlation coefficient, respectively. Seven stations were selected. The water levels in the non-flood season were also used for reference.

that multicollinearity could exist between the ISM (or WNPM) and the ISWN. The ridge regression was then applied in the solution procedure of the Multi-linear regression model, and details on this can be seen in Hoerl and Kennard (1970).

3. Results

3.1. Model validation

The simulated and observed long-term flood season water levels near or located in the frequently flooded regions are shown in Fig. 3. The results for simulated and observed water levels show that the water levels are well simulated with relative errors less than 10% and Pearson correlation coefficients larger than 0.9 at most stations. The daily Nash-Sutcliffe efficiency coefficients are all no less than 0.84 at five out seven stations. Also, the simulations of water level variation at stations (i.e., Prek Kdam and Kompong Luong) on the Tonle Sap River (TSR) and TSL indicate the reverse flow into the TSL from the Mekong River mainstem could be simulated with satisfactory performance by the hydrodynamic model that considers the backwater effect. However, the performance of water level at Can Tho and My Thuan stations is poor, where these two stations are located near the Mekong River estuary. There are two main possible explanations for this. Firstly, these two stations are strongly affected by the tide backwater effect (Peng et al., 2020), and secondly, river-bed mining in the Vietnamese Mekong Delta (VMD), which can be traced back to 1990s (Park et al., 2020), causes the water level to be reduced (Fig. 3f, the lower observed water levels after 1995 than before). These two factors were not considered in the model and thus may cause the poor performance. It is noted that the water levels at stations such as Kompong Luong and Chau Doc show obvious high values in December and the following January. This could be attributed to the release of water from the TSL in these months when the water level in the TSL is higher than the VMD (Kummu et al., 2014; Wang et al., 2021), which therefore maintains the high water levels at these stations.

The flood season spatial inundation map comparisons with MODIS and GSW are illustrated in Fig. 4. The results show that the model can capture the spatial inundation distribution well, especially in the TSL and VMD, where inundation occurs frequently during the flood season (Fig. 4). On average, 84.2% of the inundation occurrence frequency for MODIS is captured by the model in these regions (i.e., the average probability of detection is 0.842). Similar results are also obtained by using monthly GSW. It shows 88.8% of the inundation occurrence frequency of GSW is captured. Note the difference between the GSW and MODIS in the TSL regions (Fig. 4a-4b), i.e., more flooded regions are derived by GSW, potentially indicating the GSW has a better land surface waterbody detection capacity. Considering the frequently flooded regions are mainly located in the CVM, inundation analyses were therefore mainly focused on the CVM in the following sections.

Fig. 5 illustrates how the mean flood season water level changes with the monsoon index at the selected stations. It is found that the slope between the simulated water level and monsoon index is smaller than that between the observed water level and monsoon index at most stations. Nevertheless, the tendency between the mean water level and monsoon index is well captured by the model, suggesting the model can be used to characterize the monsoon impact on inundation. Also, the *p*-value calculated from the simulated water level and monsoon index is generally larger than that calculated from the observed value, indicating the threshold of *p*-value to distinguish the monsoon impact on inundation should be higher than 0.05 (or 0.10) to contain more grids in which the inundation is truly affected by the monsoon. This may prove the reasonability of the *p*-value of 0.32 as the threshold of monsoon impacts on inundation. Additionally, it is worthy to note that, though the water levels at Can Tho and My Thuan are poorly simulated, the tendency between observed mean water level and monsoon index is reproduced by the model in most cases, but with a higher slope and lower *p*-value.

3.2. Impact on inundation frequency

The impacts of monsoons on inundation frequency are shown in Fig. 6. The results show the inundation frequency mainly increases when the monsoon strengthens (i.e., a positive impact). This could be attributed to the long retention time caused by the limited flood carrying capacity. Usually, when the monsoon strengthens, then the rainfall and flood volume could be larger (Delgado et al., 2012; Yang et al., 2019). If given the unchanged flood carrying capacity, the water flow out of the

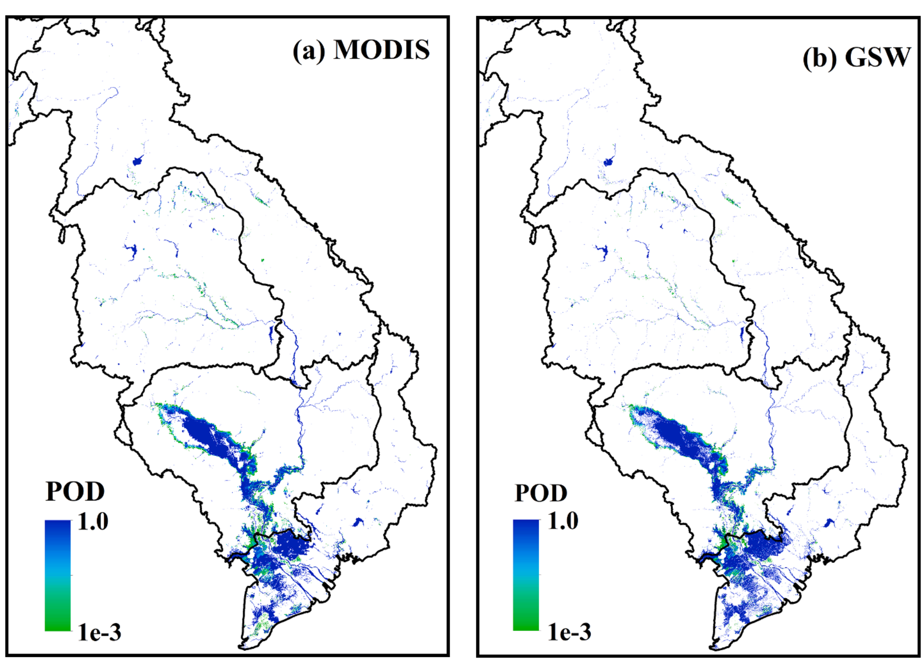

Fig. 4. The probability of detection distribution of inundation with 500 m resolution for the flood season. The daily MODIS (a) and monthly GSW (b) datasets were used and upscaled to 500 m as inundation references. Probability of detection values less than 10^{-3} were removed to show the inundation within the capacity of CaMa-Flood (i.e., the inundation that can be simulated by the model).

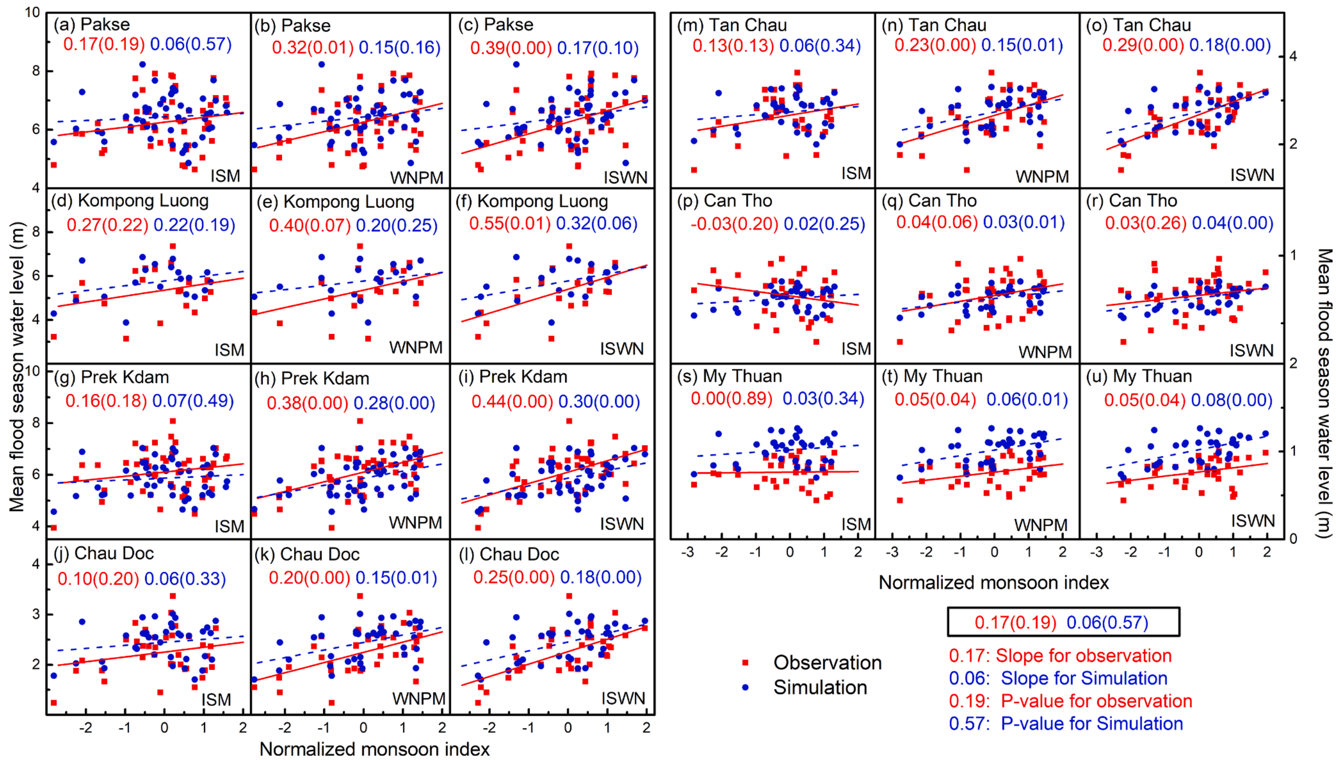

Fig. 5. The mean water level for the flood season changing with the monsoon index. The number outside the parenthesis is the slope of the fitted line in linear curve fitting, where the unit is meters. The number in the parenthesis for each slope value is the *p*-value of the Pearson correlation coefficient. In each subfigure, the location of the slope for observation is followed by that for simulation.

river cross-section could be limited, thus causing longer residence time and subsequently larger inundation frequency. For the ISM, regions showing a positive monsoon impact on inundation frequency are mainly in the outer TSL (Fig. 6a). While for the WNPM and the ISWN, regions with a positive monsoon impact on inundation frequency are mainly in the middle TSL (the inner TSL is the permanent water body), northern VMD, TSR, and the section between the Phnom Penh (i.e., confluence of the Mekong River and TSR) and Stung Treng station (hereafter abbreviated as PP-ST section). The difference in spatial distributions might be caused by the different impact areas of the monsoon on rainfall (see Yang et al., 2019; Fan and Luo, 2019; Wang et al., 2022). Further analysis of inundation pixel statistics indicates that 85.9% of the ISM impact regions have a positive monsoon impact on inundation frequency (Fig. 6a), while the percentages for the WNPM and the ISWN are 96.5% and 97.3%, respectively (Fig. 6b-6c). In the regions with a positive monsoon impact on inundation frequency, a unit increase in any one of the three monsoon indices, can lead on average to an increase of 0.03 in inundation frequency, i.e., the average slope between any one monsoon index and the inundation frequency is 0.03. When considering the percentage change of inundation frequency caused by monsoons, these increases in inundation frequency are 14.2% for the ISM, 7.7% for the WNPM, and 8.6% for the ISWN, respectively. In addition, the proportions of the region significantly affected by the monsoon (*p*-value no more than 0.05) to that affected by the monsoon (*p*-value no more than 0.32) are 17.3% for the ISM, 68.8% for the WNPM and 69.0% for the ISWN, respectively. This indicates the inundation frequency for over half of the WNPM and the ISWN impact regions is significantly affected by monsoons. In the regions significantly affected by the ISM, 89.6% of the regions show a positive monsoon impact on inundation frequency, with an average slope of 0.06 (21.8% for percentage change). For the WNPM, 99.5% of significantly affected regions have a positive monsoon impact on inundation frequency, and the average slope for these regions with a positive monsoon impact is 0.03 (6.1%). Similar results can be found for the ISWN. 99.6% of the significantly affected regions show a positive monsoon impact on inundation frequency, and in these significantly affected regions with a positive monsoon impact, a unit increase in the ISWN index can cause a 0.03 (7.2%) increase in inundation frequency.

3.3. Impact on inundation timing

Fig. 7 illustrates the monsoon impact on inundation timing at grid scale (i.e., inundation timing for depth). The results reveal that the maximum inundation depth time is mainly delayed when the ISM strengthens (i.e., a positive impact). In contrast to the ISM, the WNPM and the ISWN mainly show negative impacts on maximum inundation depth time (Fig. 7b-7c). The reason for the negative monsoon impact on maximum inundation depth time is related to the positive relationship between discharge in the southern LMRB and the WNPM (Delgado et al., 2012; Wang et al., 2022). That is, when the WNPM strengthens, the discharge inputting to the CVM system is larger, causing a higher water level outside the CVM. The maximum inundation depth time could be advanced due to the larger difference in water levels between the outside and inside of the CVM. However, due to the backwater effect in the lower regions (e.g., VMD) during the flood season, the flow of water induced by the ISM in the CVM may be greatly restricted, where discharge affected by the ISM in this region is mainly from local rainfall instead of the Mekong River mainstream (see Fan and Luo, 2019). It therefore causes a positive ISM impact on maximum inundation depth time. Further, the superposition of the positive impact of the ISM and negative impact of the WNPM can cause the impact of the ISWN on maximum inundation depth time to be either similar to the ISM or similar to the WNPM or even diminish (Fig. 7c). The regions showing a positive ISM impact on maximum inundation depth time are mainly distributed in the TSL, PP-ST section, and TSR, while those showing a negative WNPM impact on maximum inundation depth time are mainly in the TSL, TSR, northern and southern VMDs. The regions with a negative ISWN impact on maximum inundation depth time are in the southern VMD, while those with a positive ISWN impact are in the PP-ST

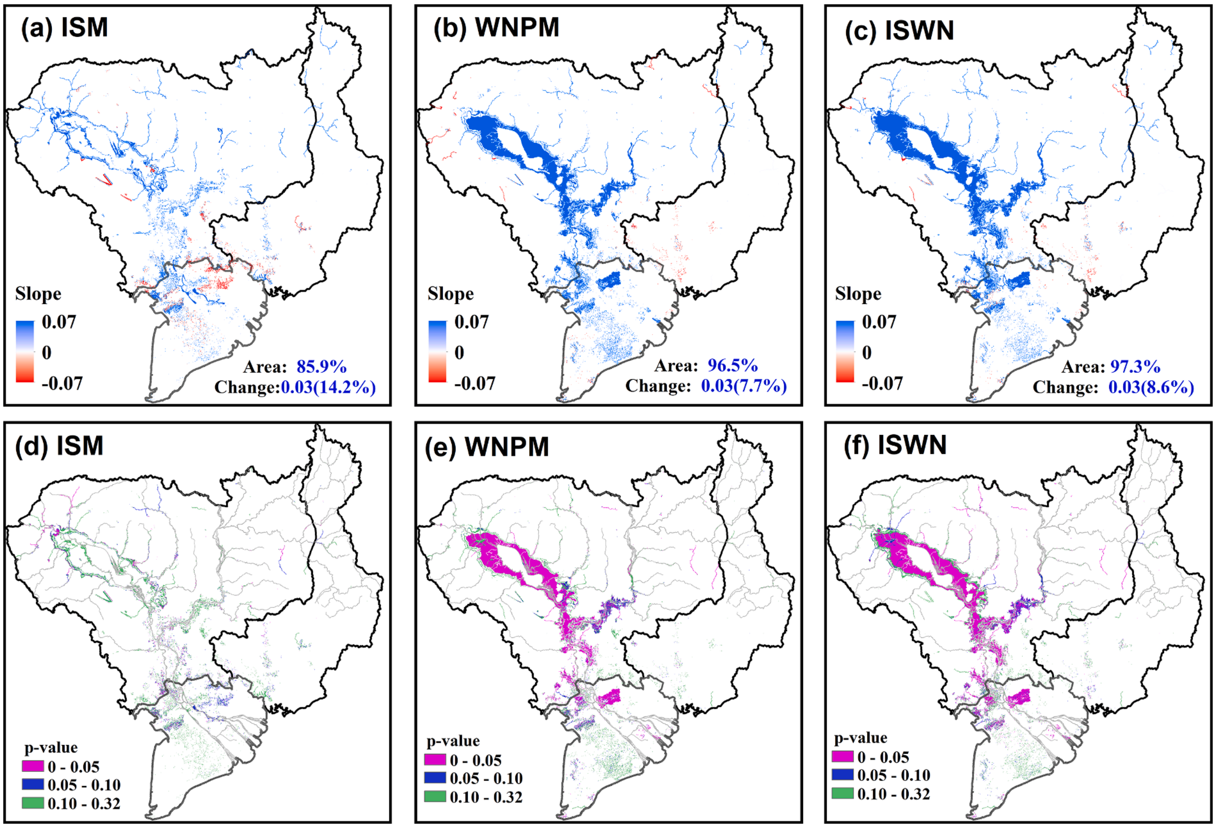

Fig. 6. The distributions of slope (a, b, c) and its corresponding *p*-value of the Pearson correlation coefficient (d, e, f) between the monsoon index and the inundation frequency. The white color indicates the regions not affected by the monsoon, while the grey lines in d-f are the rivers and permanent water bodies. The numbers for "Area" and "Change" are area percentage and average change (percentage change) of regions showing the dominant impact tendency, respectively. The unit of "Change" is the same as that of slope.

section. This spatial distribution of the ISWN impact is mainly caused by the trade-off between the impacts of the ISM and WNPM on maximum inundation depth time. 95.7% of the ISM impact regions have a positive monsoon impact on maximum inundation depth time (Fig. 7a), while the proportions for the regions showing a negative monsoon impact on maximum inundation depth time are 99.2% for the WNPM and 84.1% for the ISWN, respectively. A unit increase in the ISM index in the regions with a positive monsoon impact on maximum inundation depth time can lead to on average 4.6 days delay (1.5% change) in maximum inundation depth time, while the same change in the WNPM index in the regions with a negative monsoon impact can on average advance maximum inundation depth time by 4.3 days (1.5% change). The number for the ISWN is 5.8 days (i.e., 2.0% change). Further results show that 71.1% of the ISM impact regions are with a significant monsoon impact on maximum inundation depth time (Fig. 7d), and these values for the WNPM and the ISWN are 21.2% and 22.3%, respectively. For the ISM significant impact regions, almost all portions are with a positive monsoon impact on maximum inundation depth time, and a unit increase in ISM index can cause on average 4.4 days delay (1.4% change) in maximum inundation depth time.

3.4. Impact on inundation depth

Fig. 8 shows the monsoon impacts on average inundation depth. The results show the average inundation depth increases when the monsoon strengthens (i.e., a positive impact). This could be attributed to the larger flood volume caused by the rainy season precipitation in the years when the monsoon strengthens. The regions with a positive ISM impact on average inundation depth are mainly distributed in the outer and middle TSLs, and TSR (Fig. 8a), while the WNPM and the ISWN positively affect the average inundation depth in the TSL, PP-ST section and northern VMD (Fig. 8b-8c). The regions affected by the ISM have a proportion of 94.3% with a positive monsoon impact on average inundation depth, while the proportions with positive monsoon impacts for regions affected by the WNPM and the ISWN are 88.8% and 94.3%, respectively. For regions with a positive monsoon impact on average inundation depth, a unit increase in the ISM index can cause 0.10 m (7.0%) increase in average inundation depth, while those in the WNPM and the ISWN indices can separately cause 0.14 m (5.3%) and 0.16 m (6.7%) increases in average inundation depth. For the ISM, only 17.9% of the monsoon impact regions are with a significant monsoon impact on average inundation depth, while the numbers for the WNPM and the ISWN are 62.5% and 72.2%. Further, in the regions significantly affected by the WNPM, 98.7% of the regions have a positive monsoon impact on average inundation depth, and 0.17 m (4.9%) increase in average inundation depth can be caused by a unit increase in the WNPM index for these regions with a positive monsoon impact. For the ISWN, 99.1% of the regions significantly affected by it have a positive impact on average inundation depth, and a unit increase in its index for these regions with a positive monsoon impact can lead to 0.18 m (6.3%) increase in average inundation depth.

The monsoon impacts on maximum inundation depth are illustrated in Fig. 9. Similar impacts of the monsoon on average inundation depth can also be found on maximum inundation depth, i.e., the maximum inundation depth increases when the monsoon strengthens (a positive impact). The ISM positively affects the maximum inundation depth in the TSL, TSR and northern VMD (Fig. 9a). While for the WNPM and the ISWN, the regions showing a positive monsoon impact on maximum inundation depth include the PP-ST section besides the TSL, TSR, and northern VMD (Fig. 9b-9c). The proportions for the regions with a

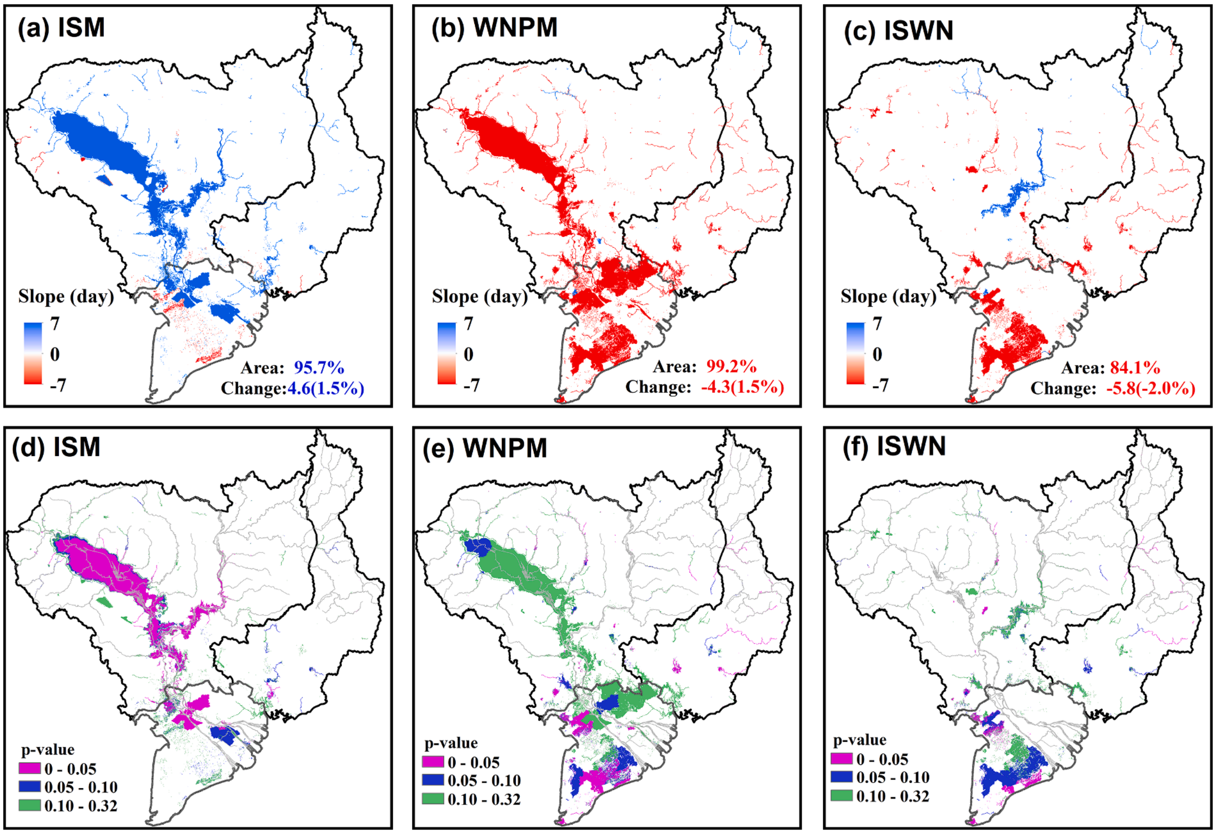

Fig. 7. The distributions of slope (a, b, c) and its corresponding *p*-value of the Pearson correlation coefficient (d, e, f) between the monsoon index and the maximum inundation depth time. The unit for slope is days.

positive monsoon impact on maximum inundation depth accounting for the monsoon impact regions are 97.2% for the ISM, 74.5% for the WNPM and 81.8% for the ISWN, respectively. In these regions with a positive monsoon impact on maximum inundation depth, a unit increase in the ISM index can lead to 0.16 m (6.8%) increase in maximum inundation depth, while those in the WNPM and ISWN indices can lead to 0.20 m (6.0%) and 0.25 m (8.1%) increases in maximum inundation depth, respectively. Also, only 12.7% of the ISM impact regions are with a significant monsoon impact on maximum inundation depth, while the numbers for the WNPM and the ISWN are 51.2% and 61.9%, respectively. 98.9% of the regions with a significant ISWN impact on maximum inundation depth have a positive monsoon impact, and 0.29 m (8.0%) increase in maximum inundation depth can be caused by a unit increase in the ISWN index for these regions with a positive monsoon impact.

3.5. Impact on inundation area

The monsoon impacts on inundation area are shown in Fig. 10, which could be regarded as a total response of flood inundation to monsoon impacts at grid scale. The results show the WNPM and the ISWN have a positive impact on the mean inundation area during the flood season (Fig. 10a, 10d, 10g), and these impacts are significant in the TSL and CVM. However, the ISM has lesser impact on the mean inundation area. The reason for the positive impact between the WNPM and mean inundation area could be the high positive correlation between the flood volume and WNPM (Delgado et al., 2012). Under the given terrain, a higher flood volume can lead to a larger inundation area. This might be also applied to the ISWN. As for the ISM, the lesser impact might be attributed to the low weight of the significantly affected regions in the regions with the ISM impact on average inundation depth (Fig. 8d). Further, a unit increase in the WNPM index can lead to increases in mean inundation area in the TSL, VMD and CVM of 3.8%, 1.0% and 2.5%, respectively. While that in the ISWN index can cause the mean inundation area in the TSL, VMD and CVM to increase by 4.3%, 1.1% and 2.7%, respectively. Except for the lesser impact of the WNPM on maximum inundation area in the VMD, almost all monsoons have a positive impact on maximum inundation area in the three considered regions. For the ISM, a unit increase in monsoon index can separately lead to 1.9%, 1.2% and 1.6% increases in maximum inundation area in the TSL, VMD and CVM. While for the WNPM, it can cause 2.8% and 1.9% increases in the TSL and CVM, respectively. Further, 3.7%, 1.4%, and 2.7% increases in maximum inundation area in the TSL, VMD and CVM can be separately caused by the ISWN when its index increases one unit.

Similar to the results of Fig. 7, the ISM has a positive impact on maximum inundation area time in the three analyzed regions, while the WNPM has a negative impact on it (Fig. 10c, 10f, 10i). The ISWN almost has no impact on maximum inundation area time. For the ISM, a unit increase in the monsoon index can delay the maximum inundation area times in the TSL, VMD and CVM by 3.7 days (1.3%), 3.8 days (1.3%), 3.2 days (1.1%), respectively. However, a unit increase in the WNPM index can separately lead to the maximum inundation area times in the TSL, VMD and CVM being advanced by 3.2 days (1.2%), 3.6 days (1.3%) and 2.8 days (1.0%).

4. Discussion

4.1. Dominant monsoon distribution

The spatial distributions of the dominant monsoon in affecting the inundation are shown in Fig. 11. The results reveal that both the WNPM and the ISWN have a larger spatial extent than the ISM in affecting inundation frequency (Fig. 11a), where they control 38.9% and 41.6% of the monsoon impact regions, respectively. The regions with a

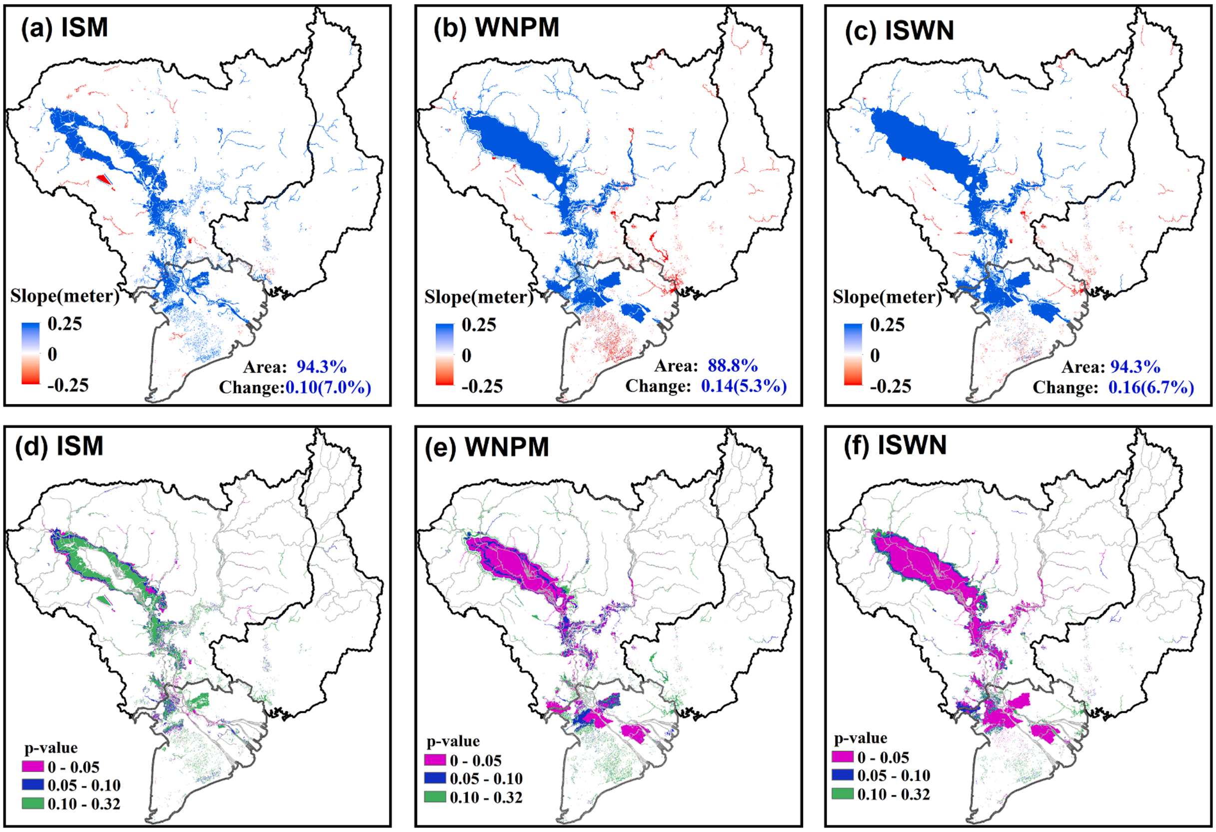

Fig. 8. The distributions of slope (a, b, c) and its corresponding *p*-value of the Pearson correlation coefficient (d, e, f) between the monsoon index and the average inundation depth during the flood season. The unit for slope is meters.

dominant ISWN impact on inundation frequency are mainly distributed in the outer and middle TSLs, and PP-ST section, while for the WNPM, the regions are mainly in the middle TSL. The ISM has the largest impact extent in affecting maximum inundation depth time (Fig. 11b), by which about 58.8% of the monsoon impact regions (e.g., TSL, TSR, PP-ST section) are mainly regulated. For inundation depth, the ISWN has the largest spatial impact extent. 70.0% of the regions with a monsoon impact on average inundation depth are mainly affected by the ISWN, while this number on maximum inundation depth is 63.7%. The regions dominated by the ISWN for the two depths are mainly in the TSL, TSR, PP-CT section and northern VMD (Fig. 11c-11d). These indicate the ISWN can have a critical role in affecting inundation, but it cannot completely replace the ISM or the WNPM, which means no monsoon can dominate the inundation alone, suggesting the spatial coexistence of three monsoons in affecting inundation. Further decomposition of the ISWN impact on inundation (i.e., ignoring the ISWN impact) shows that the WNPM has a larger spatial impact extent in affecting inundation frequency (Fig. 11e) and depth (Fig. 11g-11h), whereas the ISM has a much larger spatial impact extent in regulating the inundation timing (Fig. 11f). The regions with the WNPM impact on inundation frequency, average inundation depth and maximum inundation depth account for 72.3%, 71.0% and 74.0% of the monsoon impact regions, respectively. This number for regions with the ISM impact on maximum inundation depth time is 60.0%. In addition, the comparisons of the dominant monsoon spatial distributions before and after the ISWN decomposition show the ISWN dominant region covers most of regions that are dominated by WNPM after decomposition (e.g., Fig. 11d,11h). This could indicate many overlap regions of the ISWN and the WNPM in affecting the flood pulses and even rainfall, and can be found in Wang et al. (2022).

4.2. Monsoon contribution to inundation

The relative contributions of three monsoons to inundation are shown in Fig. 12. The results show the ISWN and the WNPM contribute similarly to inundation frequency, which are 38.8% and 39.5%, respectively. For maximum inundation depth time, the contribution of the ISM is 43.4%, while the number for the WNPM is 42.1%, which are also similar in the contribution value. The ISWN contributes most to inundation depth (Fig. 12k-12l), where its relative contributions to average inundation depth and maximum inundation depth are 43.1% and 37.2%, respectively. The contribution difference between the WNPM and the ISWN is relatively large for average inundation depth, while it is relatively small for maximum inundation depth. Further analyses of the monsoon contribution to inundation area indicate that the ISWN contributes most to the average and maximum inundation areas in the three considered regions, while the ISM contributes most to the inundation timing for area (see Fig. 10 for reference).

The ISWN was further decomposed into the ISM and WNPM, and the relative contributions of the monsoon to inundation are shown in Fig. 13. The results show the contribution of the WNPM to inundation frequency and depth is larger than that of the ISM. On average, the WNPM contributes 70.7%, 62.0%, 58.5% to inundation frequency, average inundation depth and maximum inundation depth, respectively. For the maximum inundation depth time, the WNPM contributes 54.5%, while the number for the ISM is 45.5%. In addition, the WNPM contributes more than the ISM to inundation area in most cases for the three considered regions. Nevertheless, the ISM contributes more to inundation timing for area (i.e., the day of the year that the maximum inundation area occurs, see Fig. 10 for reference).

Moreover, similar results to the dominant monsoon distribution are found by comparison of the monsoon relative contributions before and after decomposition of the ISWN, where the regions with the ISWN

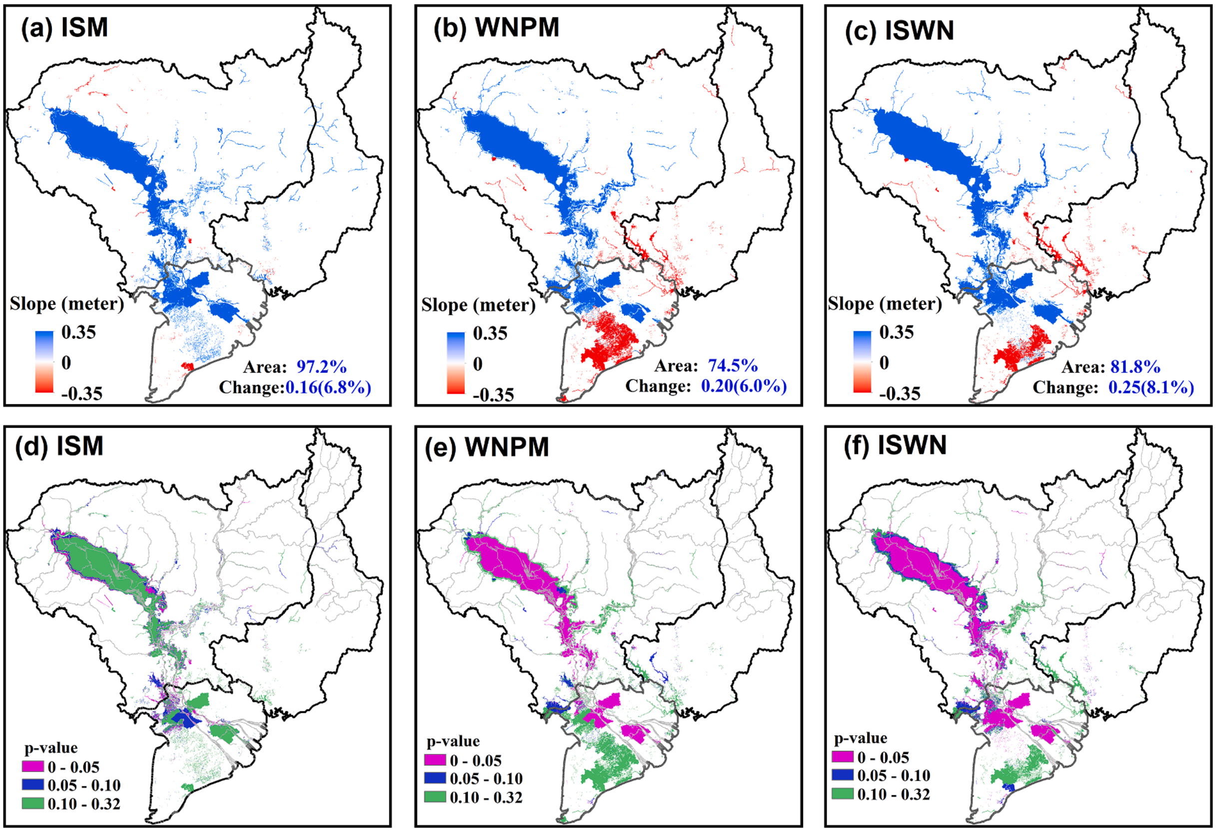

Fig. 9. The distributions of slope (a, b, c) and its corresponding *p*-value of the Pearson correlation coefficient (d, e, f) between the monsoon index and the maximum inundation depth during the flood season. The unit for slope is meters.

contributing to inundation, cover most of those with the WNPM contributing to inundation after the decomposition of the ISWN. This means the decomposition of the ISWN changes the monsoon contributions to inundation, where the WNPM contributes more to inundation, suggesting the WNPM has a larger impact than the ISM on inundation.

4.3. Uncertainty and limitation

Precipitation is the most crucial uncertainty source for the model, which affects the flood volume and thus may have some effects on the analyses of the monsoon impact on inundation. Nevertheless, the precipitation datasets used in this study were carefully selected, and one of these datasets has been proven to be one of the best datasets for hydrological modeling in the LMRB (e.g., Lauri et al., 2014; Try et al., 2020c). Moreover, the best efforts have been made to decrease the impact caused by precipitation uncertainty through model calibration. The simulated results perform well when compared with the observed values. The digital elevation map, which plays an important role in determining the inundation of a grid, is also an important source of uncertainty for the reported results. To reduce the impact caused by this uncertainty, the inundation that can be simulated by the model (i.e., within the model capacity) was considered, which could cover a large part of the real inundation. Nevertheless, a high accuracy digital elevation map is still needed to improve the quality of analyses, but this may have less influence on the results due to its invariance during the whole simulation period and the relative change of inundation being considered. In this paper, the threshold for the monsoon impact on inundation is the *p*-value of 0.32; changing the threshold can also have some impacts on the results, especially for the quantification of the monsoon impact on flood inundation. However, this will hardly change the tendency of monsoon impact on inundation.

This research only provides an initial assessment for the monsoon impact on flood inundation. The threshold for the monsoon impact on inundation (i.e., *p*-value) is worthy to be further studied, where the degree of monsoon impact can be usually underestimated by simulation (i.e., the impact exists in the observation but does not exist in the simulation, Fig. 5). Here, a lower threshold (e.g., a *p*-value of 0.05) might cause the monsoon impact regions to decrease dramatically, thus leading to the loss of much useful information (e.g., the analyses of the spatial distribution of the dominant monsoon). Since the tidal effect was not considered in the model, the inundation dynamics induced by monsoon rainfall in the southern VMD did not reproduce the observations well (Fig. 3f-3g). This is also worthy of a further study to assess the inundation separately caused by monsoon rainfall and ocean tide. It is noted that the monsoon combined effect ISWN was characterized by a simple linear combination of the ISM and the WNPM indices following Yang et al. (2019). A nonlinear superposition or linear superposition with different weights for the ISWN could have a higher correlation with precipitation and flood characteristics, and is worthy to be studied in future. In addition, the current study period covers 1967 to 2015 (i.e., 49 years in total). Extending the analytical period is also of great interest, which can provide more robust analyses.

5. Conclusions

This research used the VIC and the improved CaMa-Flood model to investigate the impacts of the ISM, the WNPM and their combined effect ISWN on flood season inundation over 1967–2015 in the LMRB. Inundation characteristics including frequency, timing, depth, and area were selected and calculated, with the slope from a linear regression model reflecting the impact of the monsoon. The spatial distribution of the dominant monsoon and monsoon relative contributions to inundation were also discussed by using a multi-linear regression model.

The water levels in the flood season at most stations were well

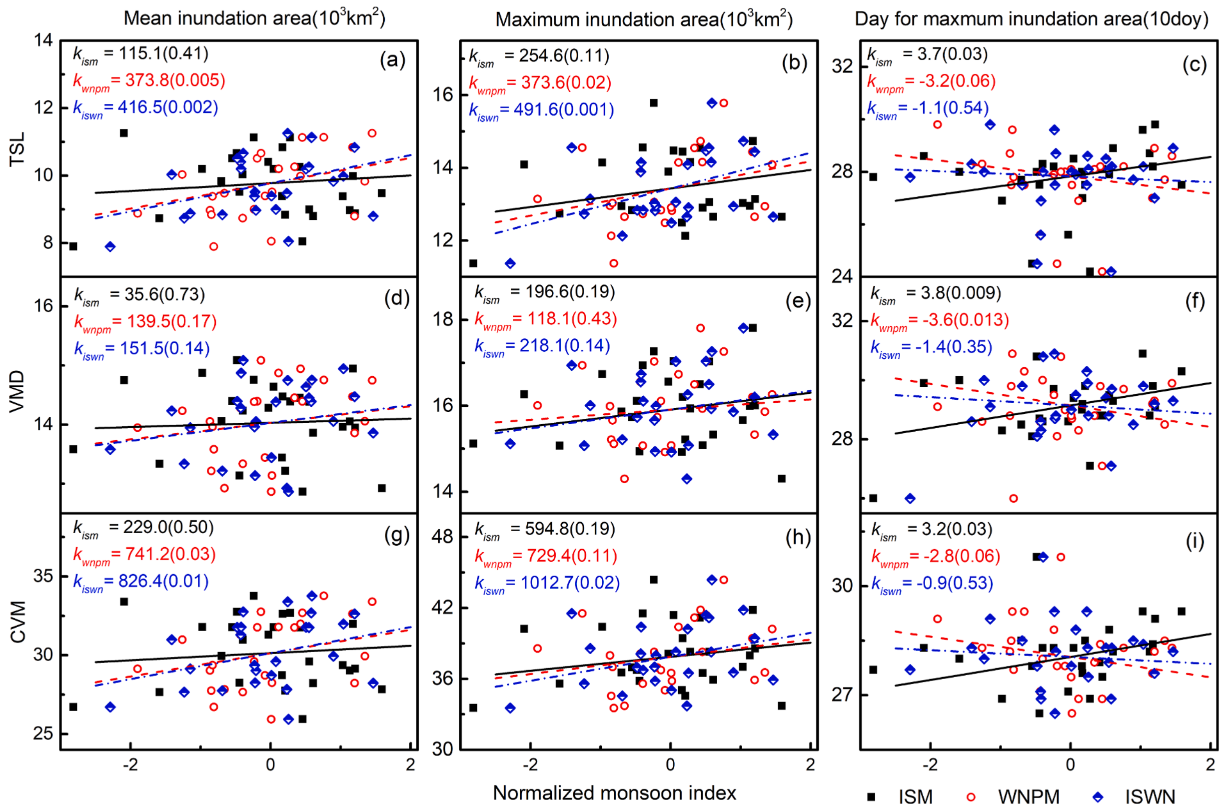

Fig. 10. Mean inundation area (a, d, g), maximum inundation area (b, e, h), and maximum inundation area time (c, f, i) varying with three normalized monsoon indices in the TSL, VMD and CVM. k is the slope of the linear curve fitting, where the units for area and date are square kilometers (km^2) and days, respectively. The number in the parenthesis for each k value is the p-value of the Pearson correlation coefficient. For research boundaries (i.e., TSL, VMD, CVM) see Fig. 1b for reference.

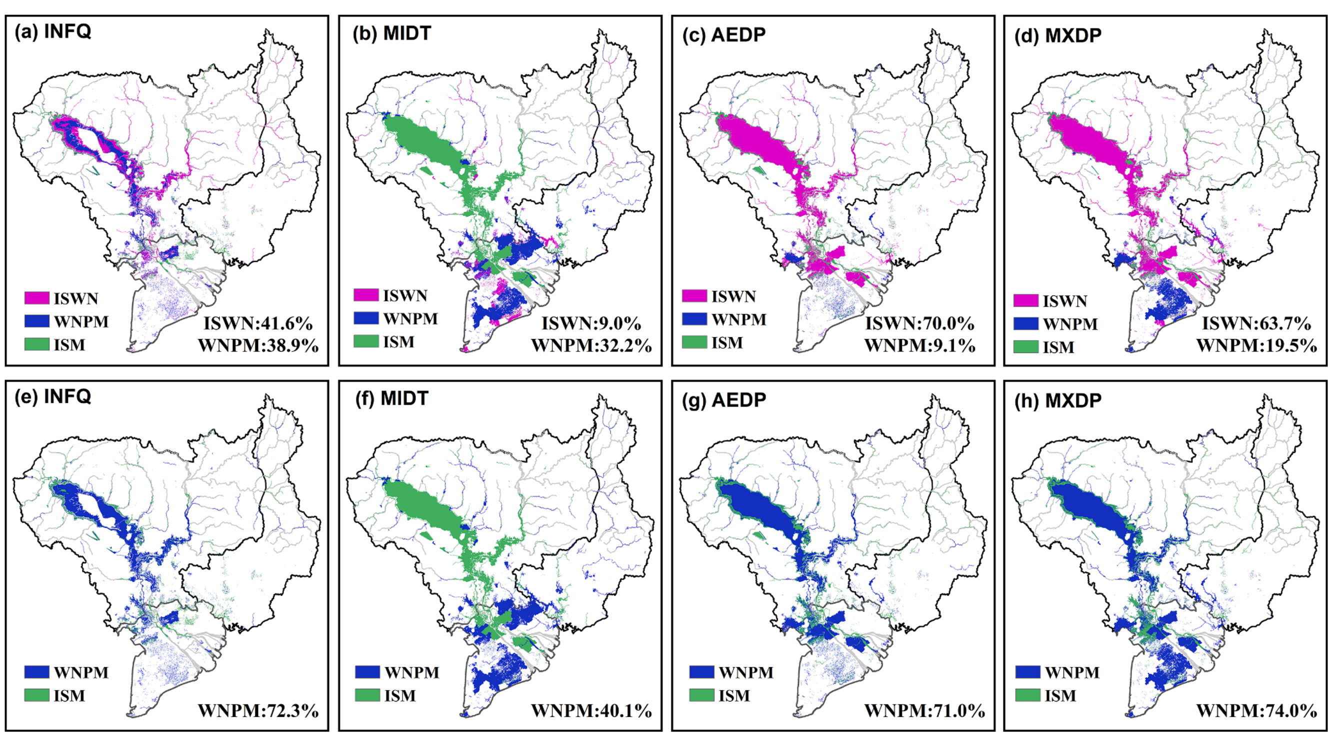

Fig. 11. The dominant regions of the ISM, WNPM and the ISWN for inundation frequency (a, e), maximum inundation depth time (b, f), average inundation depth (c, g) and maximum inundation depth (d, h). The top panel considered the ISWN, while the bottom panel decomposed the ISWN (or ignored the ISWN). The numbers in the right-bottom of each subfigure are the area percentage for the dominant monsoon.

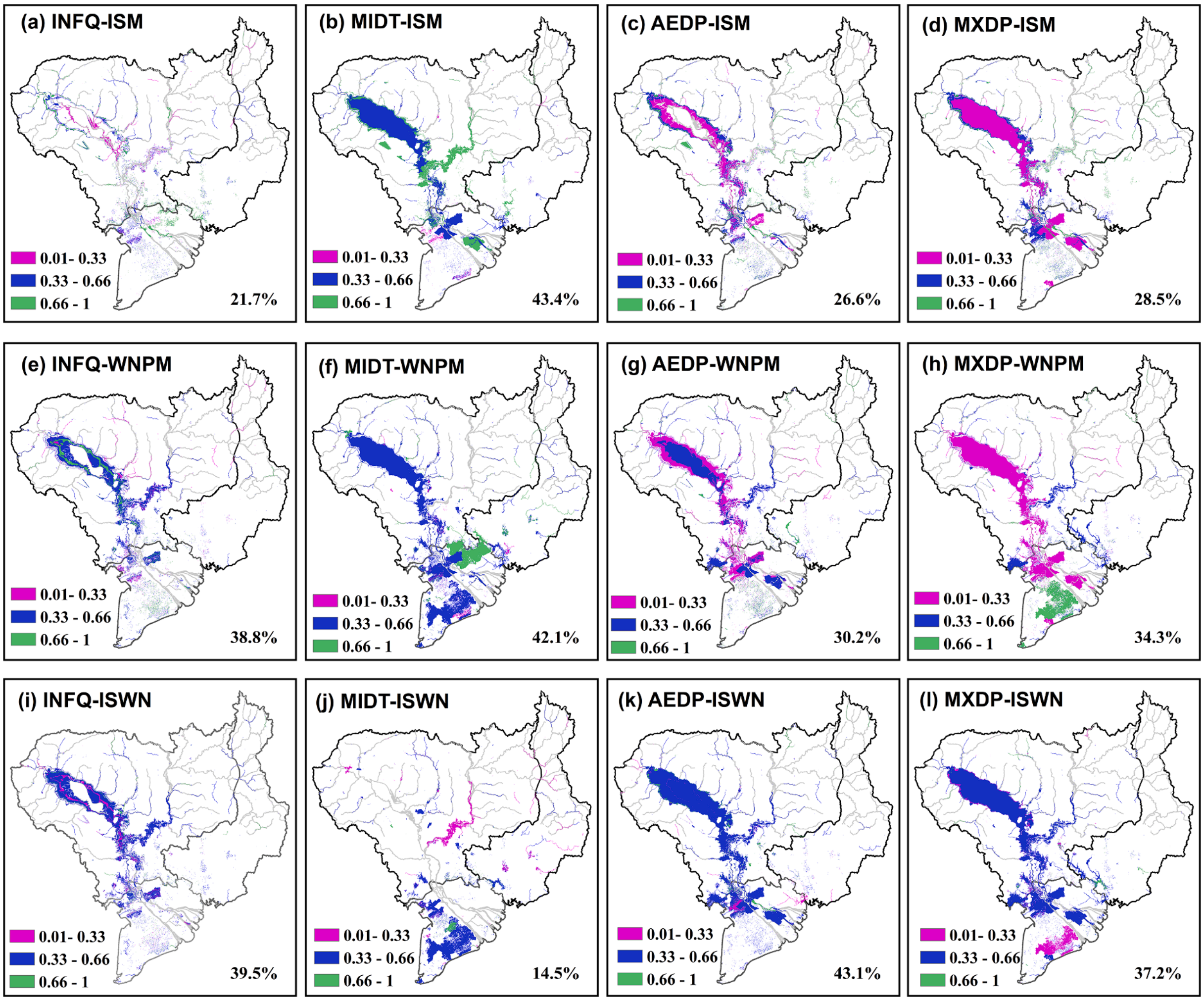

Fig. 12. The relative contributions of monsoons ISM, WNPM and ISWN to monsoon-induced inundation frequency (a, e, i), maximum inundation depth time (b, f, j), average inundation depth (c, g, k) and maximum inundation depth (d, h, l). The top, middle, and bottom panels are for the ISM, WNPM and the ISWN, respectively. The percentage in the right-bottom corner of each subfigure is the average relative contribution of monsoon.

simulated by the model. At five out seven stations, the Nash-Sutcliffe efficiency coefficients were no less than 0.84 and Pearson correlation coefficients were larger than 0.90. On average, 80%–90% of inundation occurrences were captured within the model capacity. Further results characterizing the flood season water level varying with the monsoon index indicated that the slope from the model was generally underestimated but with the same tendency.

The ISM, WNPM and the ISWN positively affected inundation frequency, depth, and area. At least 74.5% of the regions had positive monsoon impacts on frequency and depth. Further, the inundation timing for depth or area was delayed when the ISM strengthened, while it was advanced when the WNPM or the ISWN strengthened. At least 84.1% of the regions affected by the monsoon showed delayed inundation timing for depth when the ISM strengthened and advanced inundation timing for depth when the WNPM or the ISWN strengthened, respectively. For the regions with a positive monsoon impact on inundation, a unit increase in different monsoon indices could lead on average, to a 7.7%–14.2% increase in inundation frequency and 5.3%–8.1% increase in inundation depth, respectively. A unit increase in different monsoon indices could also cause a 1.0%–4.3% increase in inundation area. Moreover, a unit increase in different monsoon indices could make the inundation timing for area change by 2.8 days–3.8 days in three considered study regions, and made the inundation timing for depth on average change by 4.3 days–5.8 days.

The WNPM and the ISWN dominated the inundation frequency in over 80% of the monsoon impact regions, while the ISM dominated the inundation timing for depth in over 58% of the monsoon impact regions. Over 63% of the regions with a monsoon impact on inundation depth were mainly regulated by the ISWN. Similar contributions of the WNPM and the ISWN were detected for inundation frequency. For inundation timing for depth, the ISM and WNPM shared similar contributions, but the monsoon with the most contribution to inundation timing for area was the ISM. Moreover, the ISWN contributed most to inundation depth and area. Further decomposition of the ISWN changed the results of the impacts on inundation frequency and depth as well as area, where the WNPM contributed more to the inundation and regulated more monsoon impact regions.

CRediT authorship contribution statement

Jie Wang: Conceptualization, Methodology, Software, Writing – original draft. **Qiuhong Tang:** Conceptualization, Writing – review & editing. **Xiaobo Yun:** Writing – review & editing. **Aifang Chen:** Writing – review & editing. **Siao Sun:** Writing – review & editing. **Dai Yamazaki:** Writing – review & editing.

Declaration of Competing Interest

The authors declare that they have no known competing financial interests or personal relationships that could have appeared to influence

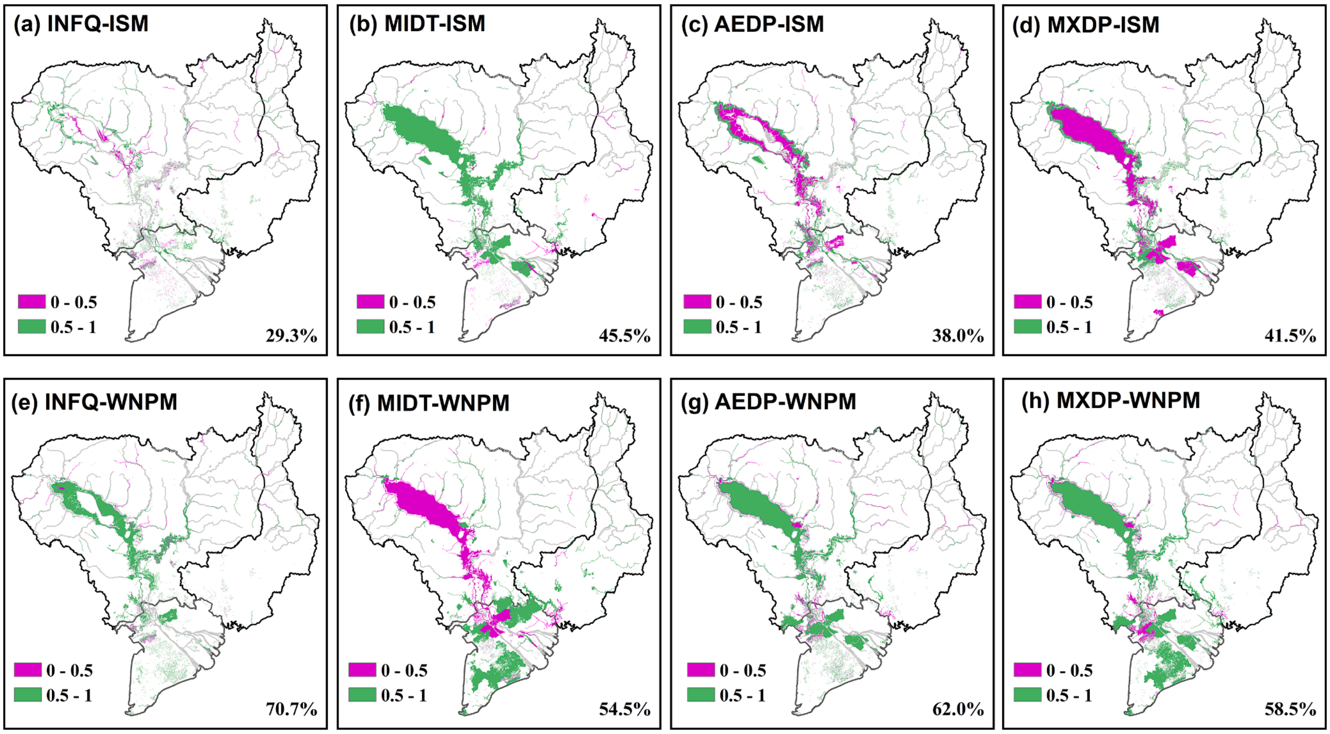

Fig. 13. The relative contributions of monsoons ISM, WNPM to monsoon-induced inundation frequency (a, e), maximum inundation depth time (b, f), average inundation depth (c, g) and maximum inundation depth (d, h). The top, bottom panels are for the ISM and WNPM, respectively. Here, the ISWN was decomposed.

the work reported in this paper.

Acknowledgements

This work was supported by the Strategic Priority Research Program of Chinese Academy of Sciences (XDA20060402), National Natural Science Foundation of China (41730645), ANSO Collaborative Research (ANSO-CR-KP-2021-09), and CAS Interdisciplinary Innovation Team (JCTD-2019-04, xbzg-zdsys-202104). Dai Yamazaki's contribution is supported by JSPS KAKENHI (21H05002). Thanks to Dr. Paul Gaffney for his comments. The CaMa-Flood model code can be obtained from http://hydro.iis.u-tokyo.ac.jp/~yamadai/, and VIC model source code is available from https://vic.readthedocs.io/en/master/. The monsoon data is obtained from http://apdrc.soest.hawaii.edu/projects/monsoon/. Parts of the discharge and Water level data are from the Mekong River Commission and Mekong River Commission website (https://portal.mrcmekong.org/, last visited on March 15, 2020). The postprocessing MODIS water body data from *Ji et al.* (2018) is available at http://data.ess.tsinghua.edu.cn/. The authors appreciate the anonymous reviewers for their valuable comments and suggestions that helped improve the manuscript.

References

Boergens, E., Dettmering, D., Seitz, F. (2019). Observing water level extremes in the Mekong River Basin: The benefit of long-repeat orbit missions in a multi-mission satellite altimetry approach. *J. Hydrol.*, *570*, 463-472.

Chen, A., Giese, M., Chen, D., 2020. Flood impact on Mainland Southeast Asia between 1985 and 2018—the role of tropical cyclones. J. Flood Risk Manag. 13 (2), e12598.

Chen, A., Liu, J., Kummu, M., Varis, O., Tang, Q., Mao, G., Wang, J., Chen, D., 2021. Multidecadal variability of the Tonle Sap Lake flood pulse regime. Hydrol. Process. 35 (9), e14327.

Costa-Cabral, M.C., Richey, J.E., Goteti, G., Lettenmaier, D.P., Feldkötter, C., Snidvongs, A., 2008. Landscape structure and use, climate, and water movement in the Mekong River basin. Hydro. Process. 22 (12), 1731–1746.

Delgado, J.M., Apel, H., Merz, B., 2010. Flood trends and variability in the Mekong river. Hydrol. Earth Syst. Sc. 14 (3), 407–418.

Delgado, J.M., Merz, B., Apel, H., 2012. A climate-flood link for the lower Mekong River. Hydrol. Earth Syst. Sc. 16 (5), 1533–1541.

Ding, Y.H., Chan, J.C., 2005. The East Asian summer monsoon: an overview. Meteorol. Atmos. Phys. 89 (1), 117–142.

Fan, X., Luo, X., 2019. Precipitation and flow variations in the Lancang-Mekong River Basin and the implications of monsoon fluctuation and regional topography. Water 11 (10), 2086.

Hameed, T., Mariño, M.A., DeVries, J.J., Tracy, J.C., 1997. Method for trend detection in climatological variables. J. Hydrol. Eng. 2 (4), 154–160.

Hoang, L.P., Lauri, H., Kummu, M., Koponen, J., van Vliet, M.T.H., Supit, I., Leemans, R., Kabat, P., Ludwig, F., 2016. Mekong River flow and hydrological extremes under climate change. Hydrol. Earth Syst. Sc. 20 (7), 3027–3041.

Hoerl, A.E., Kennard, R.W., 1970. Ridge regression: biased estimation for nonorthogonal problems. Technometrics 12 (1), 55–67.

Henck, A.C., Huntington, K.W., Stone, J.O., Montgomery, D.R., Hallet, B., 2011. Spatial controls on erosion in the Three Rivers Region, southeastern Tibet and southwestern China. Earth Planet. Sci. Lett. 303 (1–2), 71–83.

Ji, L., Gong, P., Wang, J., Shi, J., Zhu, Z., 2018. Construction of the 500-m resolution daily global surface water change database (2001–2016). Water Resour. Res. 54 (12), 10–270.

Kummu, M., Tes, S., Yin, S., Adamson, P., Józsa, J., Koponen, J., Richey, J., Sarkkula, J., 2014. Water balance analysis for the Tonle Sap Lake–floodplain system. Hydro. Process. 28 (4), 1722–1733.

Kunkel, K.E., Karl, T.R., Brooks, H., Kossin, J., Lawrimore, J.H., Arndt, D., Bosart, L., Changnon, D., Cutter, S.L., Doesken, N., Emanuel, K., Groisman, P.Y., Katz, R.W., Knutson, T., O'Brien, J., Paciorek, C.J., Peterson, T.C., Redmond, K., Robinson, D., Trapp, J., Vose, R., Weaver, S., Wehner, M., Wolter, K., Wuebbles, D., 2013. Monitoring and understanding trends in extreme storms: State of knowledge. B. Am. Meteorol. Soc. 94 (4), 499–514.

Lauri, H., Moel, H.D., Ward, P.J., Räsänen, T.A., Keskinen, M., Kummu, M., 2012. Future changes in Mekong River hydrology: impact of climate change and reservoir operation on discharge. Hydrol. Earth Syst. Sc. 16 (12), 4603–4619.

Lauri, H., Räsänen, T.A., Kummu, M., 2014. Using reanalysis and remotely sensed temperature and precipitation data for hydrological modeling in monsoon climate: Mekong River case study. J. Hydrometeorol. 15 (4), 1532–1545.

Li, F., Chen, D., Tang, Q., Li, W., Zhang, X., 2016. Hydrological response of east China to the variation of East Asian summer monsoon. Adv. Meteorol. 2016, 1–12.

Liang, X., Lettenmaier, D.P., Wood, E.F., Burges, S.J., 1994. A simple hydrologically based model of land surface water and energy fluxes for general circulation models. J. Geophys. Res-atmos. 99 (D7), 14415–14428.

Liang, X., Wood, E.F., Lettenmaier, D.P., 1996. Surface soil moisture parameterization of the VIC-2L model: Evaluation and modification. Glob. Planet. Change 13 (1–4), 195–206.

Minderhoud, P.S.J., Coumou, L., Erkens, G., Middelkoop, H., Stouthamer, E., 2019. Mekong delta much lower than previously assumed in sea-level rise impact assessments. Nat. Commun. 10 (1), 1–13.

Mohammed, I.N., Bolten, J.D., Srinivasan, R., Lakshmi, V., 2018. Satellite observations and modeling to understand the Lower Mekong River Basin streamflow variability. J. Hydro. 564, 559–573.

Park, E., Ho, H. L., Tran, D. D., Yang, X., Alcantara, E., Merino, E., Son, V. H., 2020. Dramatic decrease of flood frequency in the Mekong Delta due to river-bed mining and dyke construction. Sci. Total Environ., 723, 138066.
Pekel, J.F., Cottam, A., Gorelick, N., Belward, A.S., 2016. High-resolution mapping of global surface water and its long-term changes. Nature 540 (7633), 418–422.
Peng, H., Fok, H.S., Gong, J., Wang, L., 2020. Improving stage–discharge relation in the Mekong River Estuary by remotely sensed long-period ocean tides. Remote Sens. 12 (21), 3648.
Pokhrel, Y., Burbano, M., Roush, J., Kang, H., Sridhar, V., Hyndman, D.W., 2018. A review of the integrated effects of changing climate, land use, and dams on Mekong river hydrology. Water 10 (3), 266.
Räsänen, T.A., Kummu, M., 2013. Spatiotemporal influences of ENSO on precipitation and flood pulse in the Mekong River Basin. J. Hydro. 476, 154–168.
Sheffield, J., Goteti, G., Wood, E.F., 2006. Development of a 50-year high-resolution global dataset of meteorological forcings for land surface modeling. J. Climate 19 (13), 3088–3111.
Shin, S., Pokhrel, Y., Yamazaki, D., Huang, X., Torbick, N., Qi, J., Pattanakiat, S., Ngo-Duc, T., Nguyen, T.D., 2020. High resolution modeling of river-floodplain-reservoir inundation dynamics in the Mekong River Basin. Water Resour. Res. 56 (5).
Triet, N.V.K., Dung, N.V., Merz, B., Apel, H., 2018. Towards risk-based flood management in highly productive paddy rice cultivation–concept development and application to the Mekong Delta. Nat. Hazard. Earth Sys. 18 (11), 2859–2876.
Triet, N.V.K., Dung, N.V., Hoang, L.P., Le Duy, N., Tran, D.D., Anh, T.T., Apel, H., 2020. Future projections of flood dynamics in the Vietnamese Mekong Delta. Sci. Total Environ. 742, 140596.
Try, S., Lee, G., Yu, W., Oeurng, C., Jang, C., 2018. Large-scale flood-inundation modeling in the Mekong River basin. J. Hydrol. Eng. 23 (7), 05018011.
Try, S., Tanaka, S., Tanaka, K., Sayama, T., Lee, G., & Oeurng, C., 2020a. Assessing the effects of climate change on flood inundation in the lower Mekong Basin using high-resolution AGCM outputs. *Prog. Earth Planet. Sc.*, *7*(1), 1-16.
Try, S., Tanaka, S., Tanaka, K., Sayama, T., Hu, M., Sok, T., Oeurng, C., 2020b. Projection of extreme flood inundation in the Mekong River basin under 4K increasing scenario using large ensemble climate data. Hydro. Process. 34 (22), 4350–4364.
Try, S., Tanaka, S., Tanaka, K., Sayama, T., Oeurng, C., Uk, S., ... Han, D., 2020c. Comparison of gridded precipitation datasets for rainfall-runoff and inundation modeling in the Mekong River Basin. *Plos One*, *15*(1), e0226814.
Üneş, F., Demirci, M., Zelenakova, M., Çalışıcı, M., Taşar, B., Vranay, F., Kaya, Y.Z., 2020. River flow estimation using artificial intelligence and fuzzy techniques. Water 12 (9), 2427.
Wang, B., Wu, R., Lau, K.M., 2001. Interannual variability of the Asian summer monsoon: contrasts between the Indian and the western North Pacific-East Asian monsoons. J. climate 14 (20), 4073–4090.
Wang, J., Yun, X., Pokhrel, Y., Yamazaki, D., Zhao, Q., Chen, A., Tang, Q., 2021. Modeling Daily Floods in the Lancang-Mekong River Basin Using an Improved Hydrological-Hydrodynamic Model. Water Resour. Res. 57 (8).
Wang, J., Tang, Q., Chen, A., Tang, Y., Xu, X., Yun, X., ... Chen, D., 2022. Impacts of Summer Monsoons on flood characteristics in the Lancang-Mekong River Basin. *J. Hydro.*, 604, 127256.
Wang, W., Lu, H., Ruby Leung, L., Li, H.-Y., Zhao, J., Tian, F., Yang, K., Sothea, K., 2017. Dam construction in Lancang-Mekong River Basin could mitigate future flood risk from warming-induced intensified rainfall. Geophys. Res. Lett. 44 (20), 10,378–10,386.
Wang, Y., Feng, L., Liu, J., Hou, X., Chen, D., 2020. Changes of inundation area and water turbidity of Tonle Sap Lake: responses to climate changes or upstream dam construction? Environ. Res. Lett. 15 (9), 0940a1.
Wu, H., Adler, R.F., Tian, Y., Huffman, G.J., Li, H., Wang, J., 2014. Real-time global flood estimation using satellite-based precipitation and a coupled land surface and routing model. Water Resour. Res. 50 (3), 2693–2717.
Wu, J., Gao, X.J., 2013. A gridded daily observation dataset over China region and comparison with the other datasets (in Chinese with English abstract). China. J. Geophys. 56, 1102–1111.
Xue, Z., Liu, J.P., Ge, Q., 2011. Changes in hydrology and sediment delivery of the Mekong River in the last 50 years: connection to damming, monsoon, and ENSO. Earth Surf. Proc. Land. 36 (3), 296–308.
Yamazaki, D., de Almeida, G.A., Bates, P.D., 2013. Improving computational efficiency in global river models by implementing the local inertial flow equation and a vector-based river network map. Water Resour. Res. 49 (11), 7221–7235.
Yang, R., Zhang, W.K., Gui, S., Tao, Y., Cao, J., 2019. Rainy season precipitation variation in the Mekong River basin and its relationship to the Indian and East Asian summer monsoons. Clim. Dynam. 52 (9–10), 5691–5708.
Yatagai, A., Arakawa, O., Kamiguchi, K., Kawamoto, H., Nodzu, M.I., Hamada, A., 2009. A 44-year daily gridded precipitation dataset for Asia based on a dense network of rain gauges. Sola 5, 137–140.